Supplementary material

Epitaxial Co_2MnSi with intrinsic magnetocrystalline anisotropy as a route to bias-field-free nonlinear half-metal magnonics at the nanoscale

Anna M. Friedel[1,2,*], Jaafar Ghanbaja[2], Björn Heinz[1], Moritz Bechberger[1], Sylvie Migot[2], Sébastien Petit-Watelot[2], Stéphane Andrieu[2], Philipp Pirro[1,**]

[1] Fachbereich Physik and OPTIMAS, RPTU Kaiserslautern-Landau, Germany
[2] Institut Jean Lamour, Université de Lorraine, France

Email: *friedel@rptu.de, **ppirro@rptu.de

Cubic anisotropy

Anisotropy definition. The cubic magnetocrystalline anisotropy is best defined in the crystal coordinate system with base vectors $\{\hat{\mathbf{e}}_1 = [100], \hat{\mathbf{e}}_2 = [010], \hat{\mathbf{e}}_3 = [001]\}$ as illustrated in the main part in Figure 1a. The associated energy density up to second order reads then

$$\varepsilon_c = K_{c1} \sum_{i \neq j} (\mathbf{M} \cdot \hat{\mathbf{e}}_i)^2 \left(\mathbf{M} \cdot \hat{\mathbf{e}}_j\right)^2 + K_{c2} \prod_i (\mathbf{M} \cdot \hat{\mathbf{e}}_i)^2 \tag{S.1}$$

for $i, j = 1, 2, 3$, where K_{c1} and K_{c2} are the first and second order cubic anisotropy constants in $\mathrm{J/m^3}$.

The associated effective anisotropy field is defined via the functional derivative $\mathbf{H}_c = -\frac{1}{\mu_0}\frac{\delta \varepsilon_c}{\delta \mathbf{M}}$ and reads

$$\begin{aligned}\mathbf{H}_c = &-\frac{2K_{c1}}{\mu_0 M_{sat}^4} \sum_i \left(M_i \sum_{j \neq i} M_j^2\right) \hat{\mathbf{e}}_i \\ &-\frac{2K_{c2}}{\mu_0 M_{sat}^6} \sum_i \left(M_i \prod_{j \neq i} M_j^2\right) \hat{\mathbf{e}}_i\end{aligned} \tag{S.2}$$

where $i, j = 1, 2, 3$ and $M_{i,j} = \mathbf{M} \cdot \hat{\mathbf{e}}_{i,j}$. Following a common linearization approach[1–4], the magnetization and effective field can be written as a sum of a large static component and a small dynamic perturbation, i.e. $\mathbf{M}(\mathbf{r}, t) = \mathbf{M}_0(\mathbf{r}) + M_{sat}\delta\mathbf{m}(\mathbf{r}, t)$ and $\mathbf{H}_c = \mathbf{H}_c^{static} + \delta\mathbf{h}_c$, and keeping only the terms of lowest order in the dynamic perturbation $\delta\mathbf{m}$ allows to express the dynamic part of the anisotropy field as a linear function of the dynamic magnetisation perturbation $\delta\mathbf{m}$, i.e. $\delta\mathbf{h}_c = -\hat{N}_c \cdot M_{sat}\delta\mathbf{m}$.

Hereby the associated linearized demagnetization tensor[2–4] for the cubic magnetocrystalline anisotropy up to second order, is given by

$$\hat{N}_c = \begin{bmatrix} N_{11}^{ani} & N_{12}^{ani} & N_{13}^{ani} \\ N_{21}^{ani} & N_{22}^{ani} & N_{23}^{ani} \\ N_{31}^{ani} & N_{32}^{ani} & N_{33}^{ani} \end{bmatrix}_{123} = \hat{N}_{c1} + \hat{N}_{c2} \tag{S.3}$$

where the cubic symmetry imposes $N_{ij}^{ani} = N_{ji}^{ani}$ for $i, j = 1, 2, 3$, and explicitely

$$\hat{N}_{c1} = \frac{2K_{c1}}{\mu_0 M_{sat}^2} \begin{bmatrix} 1 - m_{01}^2 & 2m_{01}m_{02} & 2m_{01}m_{03} \\ 2m_{01}m_{02} & 1 - m_{02}^2 & 2m_{02}m_{03} \\ 2m_{01}m_{03} & 2m_{02}m_{03} & 1 - m_{03}^2 \end{bmatrix}_{123} \tag{S.4}$$

and

$$\hat{N}_{c2} = \frac{2K_{c2}}{\mu_0 M_{sat}^2} \begin{bmatrix} m_{02}^2 \cdot m_{03}^2 & 2m_{01}m_{02}m_{03}^2 & 2m_{01}m_{02}^2m_{03} \\ 2m_{01}m_{02}m_{03}^2 & m_{03}^2 \cdot m_{01}^2 & 2m_{01}^2m_{02}m_{03} \\ 2m_{01}m_{02}^2m_{03} & 2m_{01}^2m_{02}m_{03} & m_{01}^2 \cdot m_{02}^2 \end{bmatrix}_{123} \tag{S.5}$$

where $m_{0i} = \mathbf{M}_0/M_{sat} \cdot \hat{\mathbf{e}}_i$ for $i = 1, 2, 3$.

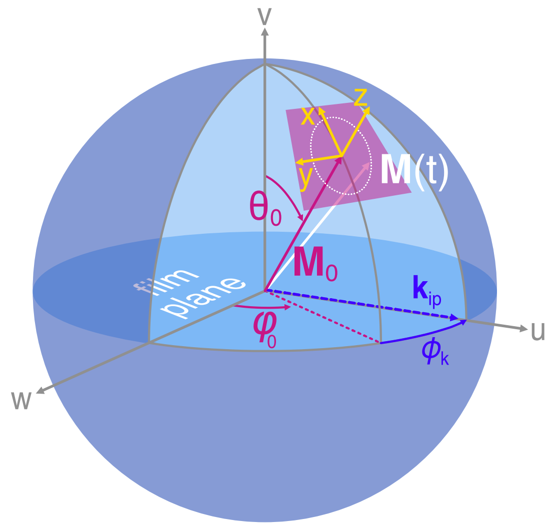

Figure S.1: Definition of the global (lab) coordinates uvw analogous to Henry *et al.*[4] and the dynamic (local) coordinates xyz used for the Kalinikos-Slavin dispersion[5,6] in Equation (S.17). The radius of the sphere is given by M_{sat}. $\mathbf{M}_0$ is the equilibrium position of the magnetisation with azimuthal and polar angles φ_0 and θ_0.

The projections m_{01}, m_{02}, m_{03} of the normalised magnetisation $\mathbf{m}_0(\mathbf{r})$ on the crystal axes can be explicitely written as

$$m_{01} = \frac{M_{01}}{M_{\text{sat}}} = \cos(\varphi_{100})\sin(\theta_{001}) \tag{S.6}$$

$$m_{02} = \frac{M_{02}}{M_{\text{sat}}} = \sin(\varphi_{100})\sin(\theta_{001}) \tag{S.7}$$

$$m_{03} = \frac{M_{03}}{M_{\text{sat}}} = \cos(\theta_{001}) \tag{S.8}$$

with the azimuthal angle $\varphi_{100} \in [0, 2\pi]$ defined with respect to $\hat{\mathbf{e}}_1 = [100]_{123}$ as illustrated in Figure 2e (main part), and the polar angle $\theta_{001} \in [0, \pi]$ (defined to $\hat{\mathbf{e}}_3 = [001]_{123}$ accordingly).

Transformation to dynamic coordinates. While the cubic magnetocrystalline anisotropy is easily expressed in the crystal coordinate system, the magnetisation dynamics in anisotropic media are typically expressed in local dynamic coordinates[2–7].

As illustrated in Figure S.1, we define the global (lab) coordinates u, v, w with base vectors $\{\hat{\mathbf{e}}_u, \hat{\mathbf{e}}_v, \hat{\mathbf{e}}_w\}$ analogous to Henry *et al.*[4], such that $\hat{\mathbf{e}}_u$ corresponds to the propagation direction and $\hat{\mathbf{e}}_v$ corresponds to the film normal. We define the local dynamic coordinates $\{\hat{\mathbf{e}}_x, \hat{\mathbf{e}}_y, \hat{\mathbf{e}}_z\}$ analogous to Kalinikos and Slavin[5,6], such that $\hat{\mathbf{e}}_\text{z} \parallel \mathbf{M}_0$ and $\hat{\mathbf{e}}_\text{y} \parallel \hat{\mathbf{e}}_\text{z} \times \hat{\mathbf{e}}_\text{v}$.

We note that in our work the film normal is fixed to the crystal axis $[001]_{\text{Co}_2\text{MnSi}}$, i.e. $\hat{\mathbf{e}}_\text{v} = \hat{\mathbf{e}}_3$. The resulting relation between local dynamic coordinates x, y, z and the crystal coordinate system for the in-plane magnetised film is illustrated in Figure 2e (main part).

The transformation from crystal coordinates $\{\hat{\mathbf{e}}_1, \hat{\mathbf{e}}_2, \hat{\mathbf{e}}_3\}$ to the dynamic coordinates $\{\hat{\mathbf{e}}_x, \hat{\mathbf{e}}_y, \hat{\mathbf{e}}_z\}$ is then given by

$$\hat{T}_{123\to xyz} = \begin{bmatrix} -\cos(\varphi_{100})\cos(\theta_{001}) & -\sin(\varphi_{100})\cos(\theta_{001}) & \sin(\theta_{001}) \\ \sin(\varphi_{100}) & -\cos(\varphi_{100}) & 0 \\ \cos(\varphi_{100})\sin(\theta_{001}) & \sin(\varphi_{100})\sin(\theta_{001}) & \cos(\theta_{001}) \end{bmatrix} \tag{S.9}$$

and allows for the transformation of the demagnetization tensor elements through

$$\hat{N}_{\text{ani}} = \begin{bmatrix} N_{xx}^{\text{ani}} & N_{xy}^{\text{ani}} & N_{xz}^{\text{ani}} \\ N_{yx}^{\text{ani}} & N_{yy}^{\text{ani}} & N_{yz}^{\text{ani}} \\ N_{zx}^{\text{ani}} & N_{zy}^{\text{ani}} & N_{zz}^{\text{ani}} \end{bmatrix}_{\text{xyz}} = \hat{T}_{123\to xyz} \cdot \begin{bmatrix} N_{11}^{\text{ani}} & N_{12}^{\text{ani}} & N_{13}^{\text{ani}} \\ N_{21}^{\text{ani}} & N_{22}^{\text{ani}} & N_{23}^{\text{ani}} \\ N_{31}^{\text{ani}} & N_{32}^{\text{ani}} & N_{33}^{\text{ani}} \end{bmatrix}_{123} \cdot \hat{T}_{123\to xyz}^{\text{T}} \tag{S.10}$$

with the transposed transformation matrix $\hat{T}_{123\to xyz}^{\text{T}}$. The transformation of $\hat{N}_\text{c}$ from Equations (S.3) to (S.5) results in a symmetric tensor $N_{ij}^{\mathrm{ani}} = N_{ji}^{\mathrm{ani}}$ for $i, j = x, y, z$ with the diagonal matrix elements

$$\begin{aligned}
N_{xx}^{\mathrm{ani}} = N_{xx}^{\mathrm{ani,c1}} + N_{xx}^{\mathrm{ani,c2}} = \frac{2K_{\mathrm{c1}}}{\mu_0 M_{\mathrm{sat}}^2} \cdot \left(1 - \frac{3}{4}\sin^2(\theta_{001})\cos^2(\theta_{001}) \cdot \left(7 + \cos(4\varphi_{100})\right)\right) \\
+ \frac{2K_{\mathrm{c2}}}{\mu_0 M_{\mathrm{sat}}^2} \cdot \sin^2(\varphi_{100})\cos^2(\varphi_{100}) \cdot \left(6\sin^2(\theta_{001}) - 20\sin^4(\theta_{001}) + 15\sin^6(\theta_{001})\right)
\end{aligned} \tag{S.11}$$

$$\begin{aligned}
N_{yy}^{\mathrm{ani}} = N_{yy}^{\mathrm{ani,c1}} + N_{yy}^{\mathrm{ani,c2}} = \frac{2K_{\mathrm{c1}}}{\mu_0 M_{\mathrm{sat}}^2} \cdot \left(1 - 6 \cdot \sin^2(\varphi_{100})\cos^2(\varphi_{100})\sin^2(\theta_{001})\right) \\
+ \frac{2K_{\mathrm{c2}}}{\mu_0 M_{\mathrm{sat}}^2} \cdot \sin^2(\theta_{001})\cos^2(\theta_{001}) \cdot \left(\frac{3}{4}\cos(4\varphi_{100}) + \frac{1}{4}\right)
\end{aligned} \tag{S.12}$$

$$\begin{aligned}
N_{zz}^{\mathrm{ani}} = N_{zz}^{\mathrm{ani,c1}} + N_{zz}^{\mathrm{ani,c2}} = \frac{2K_{\mathrm{c1}}}{\mu_0 M_{\mathrm{sat}}^2} \cdot 4\sin^2(\theta_{001}) \cdot \left(\sin^2(\varphi_{100})\cos^2(\varphi_{100})\sin^2(\theta_{001}) + \cos^2(\theta_{001})\right) \\
+ \frac{2K_{\mathrm{c2}}}{\mu_0 M_{\mathrm{sat}}^2} \cdot 15 \cdot \sin^2(\varphi_{100})\cos^2(\varphi_{100})\sin^4(\theta_{001})\cos^2(\theta_{001})
\end{aligned} \tag{S.13}$$

and the off-diagonal matrix elements

$$\begin{aligned}
N_{xy}^{\mathrm{ani}} = N_{xy}^{\mathrm{ani,c1}} + N_{xy}^{\mathrm{ani,c2}} = \frac{2K_{\mathrm{c1}}}{\mu_0 M_{\mathrm{sat}}^2} \cdot 3 \cdot \sin(\varphi_{100})\cos(\varphi_{100})\sin^2(\theta_{001})\cos(\theta_{001}) \cdot \left(\cos^2(\varphi_{100}) - \sin^2(\varphi_{100})\right) \\
+ \frac{2K_{\mathrm{c2}}}{\mu_0 M_{\mathrm{sat}}^2} \cdot \sin(\varphi_{100})\cos(\varphi_{100})\sin(\theta_{001})\cos(\theta_{001}) \\
\cdot \left(\cos^2(\varphi_{100}) - \sin^2(\varphi_{100})\right) \cdot \left(3 \cdot \sin(\theta_{001})\cos^2(\theta_{001}) - 2 \cdot \sin^3(\theta_{001})\right)
\end{aligned} \tag{S.14}$$

$$\begin{aligned}
N_{xz}^{\mathrm{ani}} = N_{xz}^{\mathrm{ani,c1}} + N_{xz}^{\mathrm{ani,c2}} = \frac{2K_{\mathrm{c1}}}{\mu_0 M_{\mathrm{sat}}^2} \cdot \sin(\theta_{001})\cos(\theta_{001}) \cdot \left(-3\cos^2(\theta_{001}) + \frac{3}{4}\sin^2(\theta_{001}) \cdot \left(\cos(4\varphi_{100}) + 3\right)\right) \\
+ \frac{2K_{\mathrm{c2}}}{\mu_0 M_{\mathrm{sat}}^2} \cdot \sin^2(\varphi_{100})\cos^2(\varphi_{100})\sin^3(\theta_{001})\cos(\theta_{001}) \\
\cdot \left(\sin^2(\theta_{001}) + 2 \cdot \left(2\sin^2(\theta_{001}) - 5\cos^2(\theta_{001})\right)\right)
\end{aligned} \tag{S.15}$$

$$\begin{aligned}
N_{yz}^{\mathrm{ani}} = N_{yz}^{\mathrm{ani,c1}} + N_{yz}^{\mathrm{ani,c2}} = \frac{2K_{\mathrm{c1}}}{\mu_0 M_{\mathrm{sat}}^2} \cdot 3 \cdot \sin(\varphi_{100})\cos(\varphi_{100})\sin^3(\theta_{001}) \cdot \left(\sin^2(\varphi_{100}) - \cos^2(\varphi_{100})\right) \\
+ \frac{2K_{\mathrm{c2}}}{\mu_0 M_{\mathrm{sat}}^2} \cdot 5 \cdot \sin(\varphi_{100})\cos(\varphi_{100})\sin^3(\theta_{001})\cos^2(\theta_{001}) \\
\cdot \left(\sin^2(\varphi_{100}) - \cos^2(\varphi_{100})\right)
\end{aligned} \tag{S.16}$$

Thin film magnetization dynamics. The Kalinikos-Slavin dispersion relation for in-plane propagating spin waves in an anisotropic thin film is given by[5,6]

$$\omega_n^2 = (\omega_{\mathrm{H}} + \omega_{\mathrm{A}}) \cdot \left(\omega_{\mathrm{H}} + \omega_{\mathrm{A}} + \omega_{\mathrm{M}}\left(F_{nn} + F_{nn}^{\mathrm{ani}}\right)\right) \tag{S.17}$$

with the dipolar matrix elements F_{nn} defined as

$$\begin{aligned}
F_{nn} = \sin^2(\theta_0) - P_{nn}\sin^2(\theta_0)\cos^2(\phi_k) \\
+ P_{nn}\left(\cos^2(\theta_0) + \frac{\omega_{\mathrm{M}}}{\omega_{\mathrm{H}} + \omega_{\mathrm{A}}}(1 - P_{nn})\sin^2(\phi_k)\sin^2(\theta_0)\right)
\end{aligned} \tag{S.18}$$

and incorporating the anisotropy energy in

$$\begin{aligned}F_{nn}^{\mathrm{ani}} &= N_{xx}^{\mathrm{ani}} + N_{yy}^{\mathrm{ani}} \\ &+ \frac{\omega_\mathrm{M}}{\omega_\mathrm{H} + \omega_\mathrm{A}} \cdot \left(N_{xx}^{\mathrm{ani}} N_{yy}^{\mathrm{ani}} + N_{yy}^{\mathrm{ani}} \sin^2(\theta_0) - \left(N_{xy}^{\mathrm{ani}}\right)^2 \right) \\ &+ P_{nn} \cdot \frac{\omega_\mathrm{M}}{\omega_\mathrm{H} + \omega_\mathrm{A}} \cdot \Big(N_{yy}^{\mathrm{ani}} \big(\cos^2(\phi_k) \\ &\qquad\qquad - \sin^2(\theta_0)\left(1 + \cos^2(\phi_k)\right)\big) \\ &\qquad + N_{xx}^{\mathrm{ani}} \sin^2(\phi_k) - N_{xy}^{\mathrm{ani}} \cos(\theta_0) \sin(2\phi_k) \Big)\end{aligned} \tag{S.19}$$

both depending on the matrix elements P_{nn} which simplify to

$$P_{00}\left(k_\mathrm{ip}\right) = 1 - \frac{1 - \exp\left(-k_\mathrm{ip} \cdot d\right)}{k_\mathrm{ip} \cdot d} \tag{S.20}$$

for the lowest order mode with mode number $n = 0$ and a homogeneous mode profile across the film thickness, i.e. $k_\mathrm{ip} \cdot d \lesssim 1$. The gyrotropic frequencies $\omega_\mathrm{M} = \gamma\mu_0 M_\mathrm{sat}$ and $\omega_\mathrm{H} = \gamma\mu_0 H_\mathrm{ext}$ are used as abbreviations to incorporate the saturation magnetisation and the external magnetic field respectively. Analogously, $\omega_\mathrm{A} = \omega_\mathrm{M} \cdot {}^{2A_\mathrm{exch}}/_{\mu_0 M_\mathrm{sat}^2} \cdot k_{n,\mathrm{tot}}^2$ is used to include the exchange interaction with exchange constant A_exch, where the total wave vector for the mode number n

$$k_{n,\mathrm{tot}}^2 = k_\mathrm{ip}^2 + k_n^2 \quad \text{with} \quad k_n = \frac{n \cdot \pi}{d} \tag{S.21}$$

is defined by its in-plane component k_ip and its quantised component along the film normal k_n with the film thickness d.

Thin film FMR. For the case of the thin-film FMR, the dispersion relation simplifies with $n = 0$ and $k_\mathrm{ip} \to 0$ to

$$\begin{aligned}\omega_\mathrm{ip}^2 = (\omega_\mathrm{H} + \omega_\mathrm{A}) \cdot \Bigg(&\omega_\mathrm{H} + \omega_\mathrm{A} + \omega_\mathrm{M}\left(1 + N_{xx}^{\mathrm{ani}} + N_{yy}^{\mathrm{ani}}\right) \\ &+ \frac{\omega_\mathrm{M}^2}{\omega_\mathrm{H} + \omega_\mathrm{A}} \left(N_{xx}^{\mathrm{ani}} N_{yy}^{\mathrm{ani}} + N_{yy}^{\mathrm{ani}} - \left(N_{xy}^{\mathrm{ani}}\right)^2 \right) \Bigg)\end{aligned} \tag{S.22}$$

for an in-plane magnetised thin film (i.e. $\theta_0 = 90°$).

The anisotropy is often incorporated in the thin film FMR formula (Kittel equation) by an anisotropy contribution aligned with the demagnetisation field, and an anisotropy contribution perpendicular to that, resulting in the factorised formula

$$\omega_\mathrm{ip}^2 = \left(\omega_\mathrm{H} + \omega_\mathrm{A} + \omega_{\mathrm{ani},y}\right) \cdot \left(\omega_\mathrm{H} + \omega_\mathrm{A} + \omega_\mathrm{M} + \omega_{\mathrm{ani},x}\right) \tag{S.23}$$

with $\omega_{\mathrm{ani},x} = -\gamma\mu_0 H_{\mathrm{ani},x}$ and $\omega_{\mathrm{ani},y} = \gamma\mu_0 H_{\mathrm{ani},y}$ for the two anisotropy contributions analogous to $\omega_\mathrm{M} = -\gamma\mu_0 H_\mathrm{demag}$ for the demagnetisation term.

The general roots of this problem

$$\omega_\mathrm{ip}^2 = \wr^2 + \wr \cdot p + q = (\wr - \wr_1) \cdot (\wr - \wr_2) \tag{S.24}$$

with $\wr = (\omega_\mathrm{H} + \omega_\mathrm{A})$ and $p = \omega_\mathrm{M}\left(1 + N_{xx}^{\mathrm{ani}} + N_{yy}^{\mathrm{ani}}\right)$ and $q = \omega_\mathrm{M}^2\left(N_{xx}^{\mathrm{ani}} N_{yy}^{\mathrm{ani}} + N_{yy}^{\mathrm{ani}} - \left(N_{xy}^{\mathrm{ani}}\right)^2\right)$ are

$$\begin{aligned}\wr_{1/2} = &-\frac{\omega_\mathrm{M}}{2}\left(1 + N_{xx}^{\mathrm{ani}} + N_{yy}^{\mathrm{ani}}\right) \\ &\pm \frac{\omega_\mathrm{M}}{2}\sqrt{\left(1 + N_{xx}^{\mathrm{ani}} - N_{yy}^{\mathrm{ani}}\right)^2 + 4\left(N_{xy}^{\mathrm{ani}}\right)^2}\end{aligned} \tag{S.25}$$

which simplifies to

$$\omega_\mathrm{ip}^2 = \left(\omega_\mathrm{H} + \omega_\mathrm{A} + \omega_\mathrm{M} N_{yy}^{\mathrm{ani}}\right) \cdot \left(\omega_\mathrm{H} + \omega_\mathrm{A} + \omega_\mathrm{M} + \omega_\mathrm{M} N_{xx}^{\mathrm{ani}}\right) \tag{S.26}$$

for $N_{xy}^{\mathrm{ani}} = 0$. This is the case for a film with the film normal $[001]_{123}$, i.e. $\theta_{001} = \frac{\pi}{2}$, for which the anisotropy tensor elements N_{xx}^{ani}, N_{xy}^{ani} and N_{yy}^{ani} simplify to

$$N_{xx}^{\mathrm{ani}} = \frac{2K_{\mathrm{c1}}}{\mu_0 M_{\mathrm{sat}}^2} + \frac{2K_{\mathrm{c2}}}{\mu_0 M_{\mathrm{sat}}^2} \cdot \sin^2(\varphi_{100}) \cos^2(\varphi_{100}) \tag{S.27}$$

$$N_{xy}^{\mathrm{ani}} = 0 \tag{S.28}$$

$$N_{yy}^{\mathrm{ani}} = \frac{2K_{\mathrm{c1}}}{\mu_0 M_{\mathrm{sat}}^2} \cdot \left(1 - 6 \cdot \sin^2(\varphi_{100}) \cos^2(\varphi_{100})\right) \tag{S.29}$$

as given in the main part in Equations (3) and (4).

Anisotropy evaluation in thin film FMR

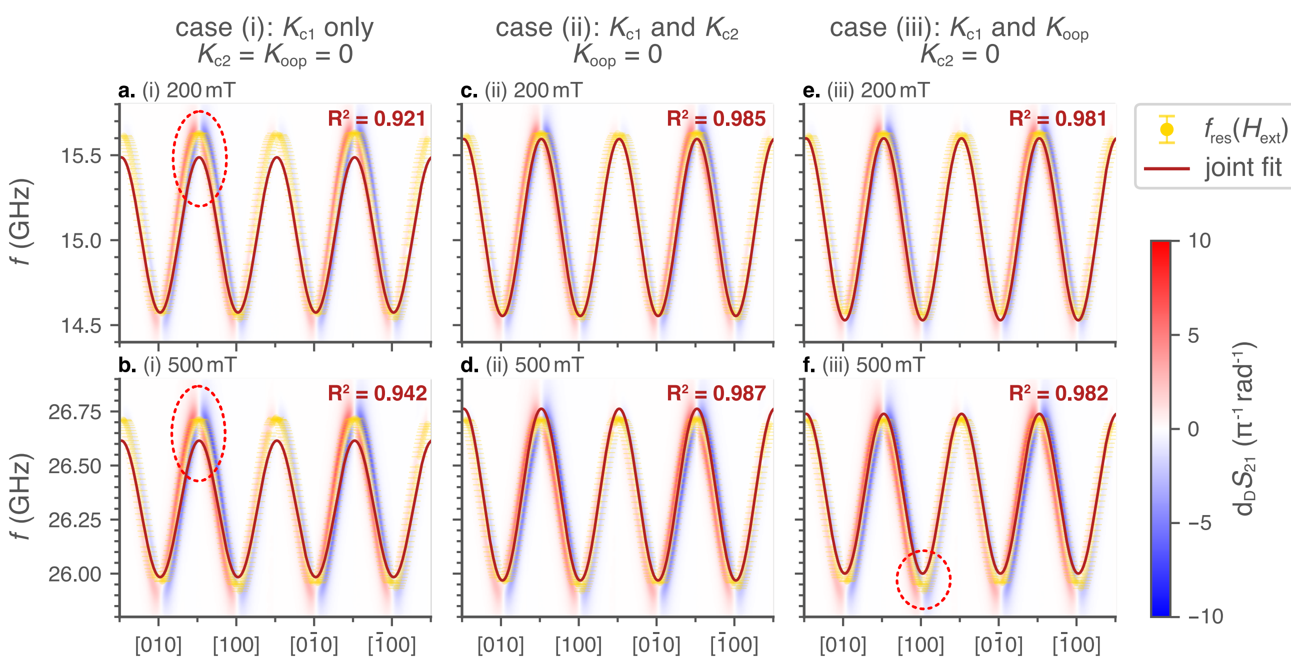

Figure S.2: Results of the fits to the rotational data from the Co_2MnSi sample for the different cases listed above. The intensity maps from the derivative divide procedure are overlayed with the resonance data points obtained from the spectral resonance curve fitting and the fit curves from the analysis procedure with the three anisotropy approaches. The red dashed circles indicate the points of significant qualitative deviations between the fit and the resonance data. The R^2 values indicated above each subpanel were calculated to determine the quality of the fit to the data shown in the respective subpanel.

Table S.1: Fit parameters corresponding to the three cases shown in Figure S.2. Note that the errors on the K_{c2} and K_{oop} are comparable: Although the absolute error on the K_{oop} is significantly lower, it amounts to 54 % of the fit parameter and is thus comparable to the 51 % relative error obtained on K_{c2}.

		(i)	(ii)	(iii)
γ	(GHz/T)	28.4 ± 0.3		
K_{c1}	(kJ/m³)	−7.9 ± 0.9	−8.1 ± 0.9	−9.2 ± 1.1
K_{c2}	(kJ/m³)	-	37.7 ± 19.4	-
K_{oop}	(kJ/m³)	-	-	−7.1 ± 3.8
$\varphi_{\mathrm{offset}}$	°	1.9 ± 1.9	1.9 ± 1.7	1.9 ± 1.7

Table S.2: Comparison of the R^2 values evaluating the match of the Kittel curves, each modelled with the best fit parameters from the three approaches as listed in Table S.1. Additionally, the average R^2 values of the Kittel fits are listed, and the R^2 values from the rotational fits in Figure S.2 are recalled.

φ_{100}	$[hkl] \parallel \mathbf{H}_{\text{ext}}$	(i)	(ii)	(iii)
0°	[100]	0.9956	0.9954	0.9956
45°	[110]	0.9930	0.9950	0.9948
90°	[010]	0.9955	0.9953	0.9955
135°	$[\bar{1}10]$	0.9935	0.9956	0.9953
180°	$[\bar{1}00]$	0.9980	0.9978	0.9981
225°	$[\bar{1}\bar{1}0]$	0.9960	0.9976	0.9974
270°	$[0\bar{1}0]$	0.9978	0.9977	0.9979
315°	$[1\bar{1}0]$	0.9969	0.9982	0.9980
average ip-Kittel		0.9958	0.9966	0.9966
200 mT rotational		0.9210	0.9851	0.9810
500 mT rotational		0.9421	0.9870	0.9818
oop-Kittel		-	0.958	0.791

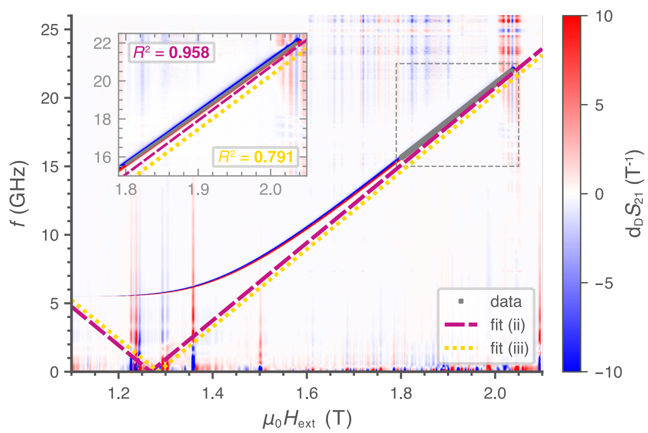

Figure S.3: Fit results for case (ii) and case (ii) modelled to the out-of-plane data set. The inset shows a zoom-in on the area marked by the dashed rectangle additionally indicating the obtained R^2 values evaluating the match of the two models to the high-field data, i.e. for $\mu_0 H_{\text{ext}} > 1.8\,\text{T}$, for which the spectral resonance data positions (obtained from the spectral resonance curve fitting) are indicated by the grey cross markers.

Linewidth evaluation

Table S.3: Linewidth analysis on the in-plane Kittel datasets (see Figure S.4 hereafter).

φ_{100}	$[hkl] \parallel \mathbf{H}_{\text{ext}}$	$\alpha(10^{-3})$	$\mu_0 \Delta H_0$(mT)
0°	[100]	1.271±0.01	0.835±0.01
45°	[110]	1.106±0.01	1.071±0.01
90°	[010]	1.192±0.01	0.771±0.01
135°	$[\bar{1}10]$	1.115±0.01	1.011±0.01
average	$\langle 110 \rangle$	1.23±0.01	0.80±0.01
average	$\langle 100 \rangle$	1.11±0.01	1.04±0.01
average all		1.17±0.01	0.92±0.01

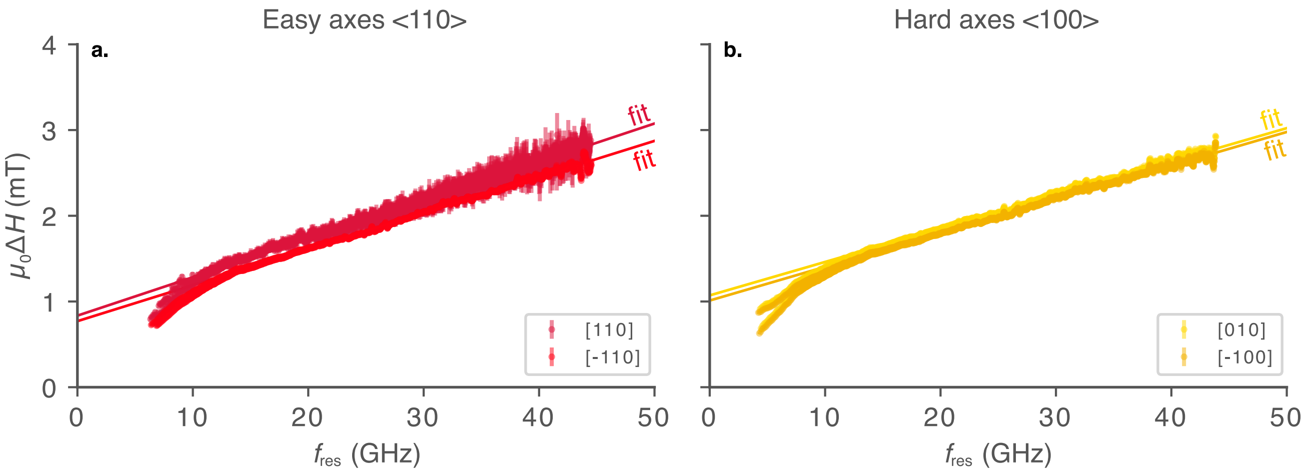

Figure S.4: Linewidth analysis on the in-plane Kittel datasets. Resonance linewidths (HWHM) extracted from the spectral resonance curve fits from the Co_2MnSi film and transformed to field linewidths $\mu_0\Delta H_{res}$ for (a) the field oriented along the $\langle 110\rangle$ directions (easy axes) and (b) the $\langle 100\rangle$ directions (hard axes). The lines represent fits with the function $\mu_0\Delta H_{res} = \mu_0\Delta H_0 + \frac{\alpha\cdot\omega_{res}}{\gamma}$, which was fitted to the data with $20\,\mathrm{GHz} \leq f_{res}$.

References

(1) Hillebrands, B. *Physical Review B* **1990**, *41*, 530–540, DOI: 10.1103/PhysRevB.41.530.

(2) Patton, C. E. *physica status solidi (b)* **1979**, *92*, 211–220, DOI: 10.1002/pssb.2220920124.

(3) Patton, C. E. *physica status solidi (b)* **1979**, *93*, 63–69, DOI: 10.1002/pssb.2220930106.

(4) Henry, Y.; Gladii, O.; Bailleul, M. Propagating Spin-Wave Normal Modes: A Dynamic Matrix Approach Using Plane-Wave Demagnetizating Tensors, 2016, DOI: 10.48550/ARXIV.1611.06153.

(5) Kalinikos, B. A.; Slavin, A. N. *Journal of Physics C: Solid State Physics* **1986**, *19*, 7013–7033, DOI: 10.1088/0022-3719/19/35/014.

(6) Kalinikos, B. A.; Kostylev, M. P.; Kozhus, N. V.; Slavin, A. N. *Journal of Physics: Condensed Matter* **1990**, *2*, 9861–9877, DOI: 10.1088/0953-8984/2/49/012.

(7) Körber, L.; Quasebarth, G.; Otto, A.; Kákay, A. *AIP Advances* **2021**, *11*, 095006, DOI: 10.1063/5.0054169.